Geophysical Research Letters

RESEARCH LETTER
10.1029/2021GL097234

Potential Impact of Spring Thermal Forcing Over the Tibetan Plateau on the Following Winter El Niño–Southern Oscillation

Wei Yu[1,2], Yimin Liu[3,4], Lianlian Xu[1,2], Guoxiong Wu[3,4], Song Yang[1,2], Dake Chen[1,5,6], Xiu-Qun Yang[7], Chundi Hu[1,2], and Bian He[3,4]

[1]School of Atmospheric Sciences, Sun Yat-sen University, Southern Marine Science and Engineering Guangdong Laboratory (Zhuhai), Zhuhai, China, [2]Guangdong Province Key Laboratory for Climate Change and Natural Disaster Studies, Sun Yat-sen University, Zhuhai, China, [3]State Key Laboratory of Numerical Modeling for Atmospheric Sciences and Geophysical Fluid Dynamics, Institute of Atmospheric Physics, Chinese Academy of Sciences, Beijing, China, [4]University of Chinese Academy of Sciences, Beijing, China, [5]State Key Laboratory of Satellite Ocean Environment Dynamics, Second Institute of Oceanography, Ministry of Natural Resources, Hangzhou, China, [6]School of Oceanography, Shanghai Jiao Tong University, Shanghai, China, [7]China Meteorological Administration–Nanjing University Joint Laboratory for Climate Prediction Studies, School of Atmospheric Sciences, Nanjing University, Nanjing, China

Abstract Using observational analysis and numerical experiments, we identify that the dipole mode of spring surface wind speed (SWS) over the Tibetan Plateau (TP) could act as a trigger for subsequent winter El Niño–Southern Oscillation events. During the positive phase of spring SWS dipole mode (south-positive and north-negative), a self-sustaining "negative sensible heating–baroclinic structure" prevails over the western TP, which is characterized by negative surface sensible heating anomalies, anomalous low-level anticyclones, and mid–high-level cyclones. The "negative sensible heating–baroclinic structure" stimulates the surface westerly wind anomalies over the tropical western Pacific in May through two pathways, favoring the occurrence of subsequent El Niño events. One is through weakening the zonal monsoon circulation over the tropical Indian Ocean and the Walker circulation over the tropical western Pacific. The other is modulating the air–sea interaction over the North Pacific through triggering Rossby waves. The negative SWS dipole mode tends to induce La Niña events.

Plain Language Summary El Niño–Southern Oscillation (ENSO) can exert pronounced climate impacts over the tropical Pacific and other remote regions. Meanwhile, the occurrence of ENSO events is also affected by local tropical Pacific and non-local factors. As an elevated, huge, and intense heat source over the subtropics, Tibetan Plateau (TP) thermal forcing exerts significant influences on atmospheric circulations and oceans across the whole globe. This study explores the impact of spring TP thermal forcing on the formation of ENSO in following winter. In the observations, the south–north dipole modes of spring surface sensible heating and surface wind speed over the TP can stimulate the surface zonal wind anomalies over the tropical western Pacific in May through two pathways, favoring the occurrence of subsequent ENSO events. One is through influencing the zonal monsoon circulation over the tropical Indian Ocean and the Walker circulation over the tropical western Pacific. The other is modulating the air–sea interaction over the North Pacific through triggering Rossby waves. These two pathways are well reproduced in numerical experiments.

Key Points:

- Spring positive surface wind speed (SWS) dipole mode over Tibetan Plateau is closely connected with a "negative sensible heating-baroclinic structure"
- Spring positive SWS dipole mode induces winter El Niño by modulating surface westerly wind anomalies over tropical western Pacific in May
- Surface westerly wind anomalies over tropical western Pacific in May are induced through gearing between the Indian and Pacific oceans and seasonal footprinting mechanism processes

Supporting Information:

Supporting Information may be found in the online version of this article.

Correspondence to:

Y. Liu,
lym@lasg.iap.ac.cn

Citation:

Yu, W., Liu, Y., Xu, L., Wu, G., Yang, S., Chen, D., et al. (2022). Potential impact of spring thermal forcing over the Tibetan Plateau on the following winter El Niño–Southern Oscillation. *Geophysical Research Letters*, *49*, e2021GL097234. https://doi.org/10.1029/2021GL097234

Received 11 DEC 2021
Accepted 22 FEB 2022

1. Introduction

El Niño–Southern Oscillation (ENSO) is a large-scale air–sea interaction phenomenon, which is characterized by sea surface temperature (SST) anomalies (SSTAs) over the tropical central-eastern Pacific, accompanied by surface pressure oscillation between the tropical eastern Pacific and the western Pacific (Bjerknes, 1969). As the strongest interannual variability signal in the global climate system, ENSO exerted substantial impacts on the weather and climate over the surrounding areas and even across the globe through oceanic processes and atmospheric teleconnections (Alexander et al., 2002; McPhaden et al., 2006; Trenberth, 1997; B. Wang et al., 2000). A substantial body of work had been conducted for comprehensive understandings of the formation of ENSO events (Bjerknes, 1969; Jin, 1997; Schopf & Suarez, 1988; C. Z. Wang, 2001; Weisberg & Wang, 1997; Wyrtki, 1985). Overall, factors originated in the tropical Pacific could serve as triggers for the occurrence of ENSO events, which mainly include the sustained tropical western Pacific westerly wind bursts (Eisenman et al., 2005; Fedorov

et al., 2015; Lian et al., 2014; McPhaden, 1999), the intensity of tropical Pacific trade winds (Guilyardi, 2006), the zonal-averaged thermocline depth (Latif et al., 1993), and the zonal SST gradient (Knutson et al., 1997).

Numerous remote climate systems could also stimulate ENSO events through modulating the surface westerly wind bursts in the tropical western Pacific. For example, Wu and Meng (1998) found that the zonal monsoon circulation over the equatorial Indian Ocean and the Walker circulation over the equatorial Pacific were closely coupled. When one moved clockwise and the other moved anticlockwise, this pattern was referred to as the "gearing between the Indian and Pacific oceans (GIP)". They also pointed that when the GIP was in the negative rotation, the Asian summer monsoon circulation and Walker circulation were weakened, and surface westerly wind bursts occurred in the tropical western Pacific, which was in favor of the occurrence of El Niño events in winter. Moreover, the winter North Pacific Oscillation could also modulate the occurrence of ENSO events through influencing the surface westerly wind bursts over the tropical western Pacific. This process was named as the seasonal footprinting mechanism (SFM; Vimont et al., 2001, 2003).

The Tibetan Plateau (TP) acts as an elevated, huge, and intense heat source over the subtropical central-eastern Eurasian continent, which could regulate the tropical atmospheric and oceanic systems through the uplift and thermal forcing (Duan & Wu, 2005; Liu et al., 2007, 2020; Sun et al., 2019; B. Wang et al., 2008; Wen et al., 2020; Wu et al., 1997, 2007). Wen et al. (2020) revealed that without the TP, the tropical Pacific trade winds would weaken, the mixed layer would become shallow, and the El Niño–like SST would occur more frequently. Previous studies had shown that the upper-level warming over the TP in summer could induce the Asian–Pacific Oscillation atmospheric teleconnection, which could affect the appearance of La Niña events via modulating the intensity of the Pacific subtropical high (Nan et al., 2009; P. Zhao et al., 2007). In addition to these limited studies, how TP thermal forcing affects ENSO events still warrant further investigation.

Surface sensible heating (SH) is the most dominant source of diabatic heating during spring over the TP (Duan & Wu, 2008; Y. Zhao et al., 2018). It exerted substantial impacts on the onset and intensity of the Asian summer monsoon via its air pump effect (Wu et al., 1997, 2007), and on the downstream North Pacific by triggering Rossby waves (Sun et al., 2019). However, it is still unclear whether the spring SH over the TP can affect the ENSO events in subsequent winter. In previous study, we showed that the first and second leading empirical orthogonal function (EOF) modes of spring SH over the TP were separately characterized by a uniform mode and a south–north dipole mode on the interannual timescale, which were closely related to the simultaneous TP surface wind speed (SWS) (Yu et al., 2021). In this paper, we would provide sufficient evidences to reveal that the south–north dipole mode of spring SWS over the TP could serve as a trigger for the subsequent winter ENSO events based on observations and numerical simulations. This study might be beneficial for improving the prediction skill of wintertime ENSO events.

2. Data and Model

2.1. Data

The monthly mean heat fluxes and circulation data are provided by the Modern-Era Retrospective Analysis for Research and Applications version 2 (MERRA-2, 0.625° × 0.5°, Gelaro et al., 2017). The monthly mean precipitation data are derived from the Global Precipitation Climatology Project version 2.3 (GPCP2.3, 2.5° × 2.5°, Adler et al., 2003). The monthly mean SST data from the Hadley Centre Sea Ice and SST Data Set version 1 (HadISST1, 1° × 1°, Rayner et al., 2003) and the monthly mean potential temperature from Global Ocean Data Assimilation System (GODAS, 1/3° × 1°, Behringer & Xue, 2004) are also employed.

All the above datasets cover the period from 1980 to 2014. This study focuses on the interannual timescale. The linear trends of all the monthly mean variables are removed, and then the 2–9-year bandpass Lanczos filter are conducted on the detrended variables to extract the interannual components (Duchon, 1979). The four seasons are spring (March–May, MAM), summer (June–August, JJA), autumn (September–November, SON), and winter (December–February, DJF). The wave activity flux is employed to diagnose the propagation of Rossby waves (Takaya & Nakamura, 2001). The Niño3.4 index (area-averaged SSTAs over 5°S–5°N, 170°–120°W) is utilized to represent the intensity of ENSO events. The statistical significance of the correlation and regression coefficients are estimated based on the two-tailed Student's *t*-test.

2.2. Model

The Flexible Global Ocean–Atmosphere–Land System Model, finite volume version 2 (FGOALS-f2) is employed in this study, which is developed by the State Key Laboratory of Numerical Modeling for Atmospheric Sciences and Geophysical Fluid Dynamics, Institute of Atmospheric Physics, Chinese Academy of Sciences, Beijing, China (Bao et al., 2013, 2019). The horizontal resolution of the ocean, land, and atmosphere is about 1° × 1°. The FGOALS-f2 participated in the Coupled Model Intercomparison Project Phase 6 (CMIP6, B. He, Bao, et al., 2019). It showed good performance in representing the characteristics of ENSO, the propagation of the Madden–Julian Oscillation, and precipitation over the TP and East Asia (Bao et al., 2013, 2019; S. C. He, Yang, et al., 2019; Li et al., 2019).

2.3. Numerical Experiments Design

Two experiments are designed in this study. The control run (CTRL) is a freely coupled ocean–atmosphere–land general circulation model experiment, which integrates for 100 years, and only the last 20 years are analyzed. The sensitivity experiments include 20 members, which integrate from 21 April to 31 December with the same temperature anomalies forcing (hereafter referred to as TP–T). The initial fields in 20 members of TP–T experiments are taken from every 21 April of the last 20 years in the CTRL experiment. Each TP–T experiment is forced by the linearly decreasing temperature anomalies from 21 April (0°C) to 30 April (minimum value), and retains its minimum value during 1–31 May. The horizonal distribution of the temperature anomalies linearly decrease from the outermost ellipse (0°C) to its center (28°N, 68°E) (Figure 2f). The vertical distribution of the center is the negative temperature anomalies with two cold centers (−3°C) at the surface and 325 hPa (Figure S8a in the Supporting Information S1), which is similar to the distribution in Figure 2e. The difference between ensemble means of TP–T and CTRL is evaluated.

3. Results

3.1. Connections Between Spring SWS Over the TP and ENSO on the Interannual Timescale

According to the bulk aerodynamic formula (Duan & Wu, 2008), the SH is largely determined by the SWS and the surface land–air temperature difference (Ts–Ta). On the interannual timescale, the Ts–Ta is less important than the SWS to the variation of spring SH over the TP (Duan & Wu, 2008; Yu et al., 2018). Here we investigate the first two leading EOF modes of interannual SWS and SH over the main body of TP and their corresponding time series (SWSPC1, SWSPC2, SHPC1, SHPC2, Figures 1 and S1 in the Supporting Information S1). This main body of TP is defined as regions with altitude higher than 2,000 m, which has been widely adopted in many previous researches (Duan & Wu, 2008; Sun et al., 2019). The spatial patterns of the EOF1 of both SWS and SH are uniform over the TP (Figures S1e and S1a in the Supporting Information S1), and their time series are highly correlated ($r = 0.68$, $p < 0.01$). The EOF2 of these two variables show south–north dipole patterns (Figures 1a and S1c in the Supporting Information S1) and the correlation coefficient between SWSPC2 and SHPC2 is 0.35 ($p < 0.05$). Previously, we found that the variation of SH was not consistent among station data, MERRA-2, JRA-55, and ERA-Interim reanalysis data, while the variation of SWS was consistent among them (Yu et al., 2021). For above reasons, the SWS is employed as a good proxy for the SH over the TP in this study.

The spring SWSPC1 shows a weak positive relationship with the preceding winter Niño3.4 index ($r = 0.25$, $p > 0.1$) and a weak negative relationship with the subsequent winter Niño3.4 index ($r = -0.24$, $p > 0.1$) (Figure S2 in the Supporting Information S1). Since the EOF2 of SWS shows a south–north dipole pattern, an index (SWS dipole (SWSD)) is defined as the difference of averaged SWS between the south box and north box (Figure 1a), which is highly connected with SWSPC2 ($r = 0.94$, $p < 0.01$, Figure 1b). The spring SWSD shows insignificant relationship with the preceding winter Niño3.4 index ($r = -0.27$, $p > 0.1$, Figure S3a in the Supporting Information S1), but exhibits remarkably positive correlations with subsequent autumn ($r = 0.41$, $p < 0.05$, Figure 1c) and winter Niño3.4 index ($r = 0.46$, $p < 0.01$, Figure 1d). That is, the relationship between EOF1 of spring SWS and ENSO is insignificant, while the EOF2 of spring SWS is closely connected to the following ENSO. The spring SWSD accounts for about 21% variance of the succeeding winter ENSO variability. In this paper, we are trying to point out that the spring SWS dipole mode over the TP is an important but not the only factor for inducing the subsequent winter ENSO events.

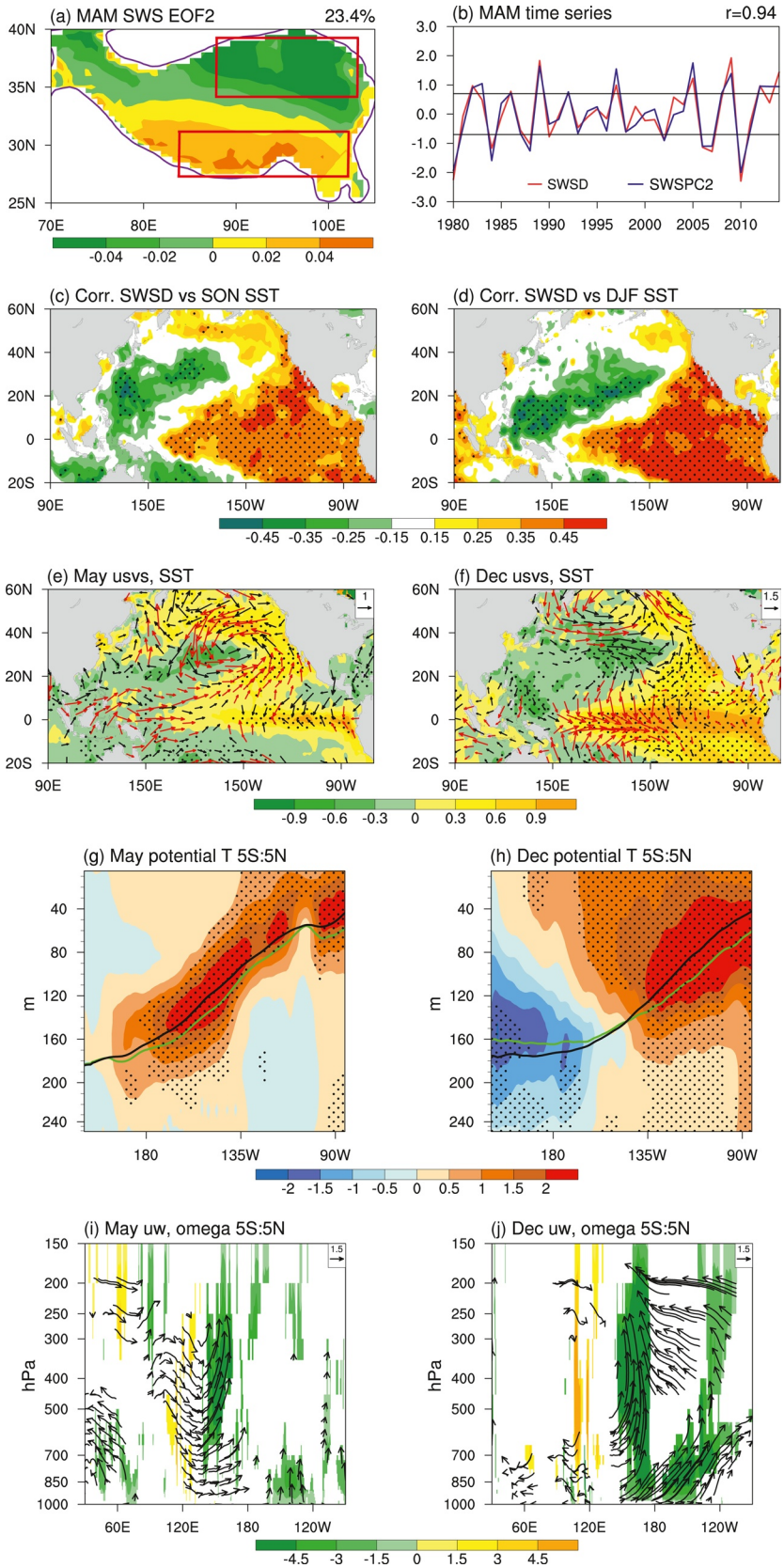
(a) MAM SWS EOF2
23.4%
40N
35N
30N
25N
70E
80E
90E
100E
-0.04 -0.02 0 0.02 0.04
(b) MAM time series
r=0.94
3.0
2.0
1.0
0.0
-1.0
-2.0
-3.0
SWSD
SWSPC2
1980 1985 1990 1995 2000 2005 2010
(c) Corr. SWSD vs SON SST
(d) Corr. SWSD vs DJF SST
60N
40N
20N
0
20S
90E 150E 150W 90W
-0.45 -0.35 -0.25 -0.15 0.15 0.25 0.35 0.45
(e) May usvs, SST
(f) Dec usvs, SST
1
1.5
-0.9 -0.6 -0.3 0 0.3 0.6 0.9
(g) May potential T 5S:5N
(h) Dec potential T 5S:5N
m
40
80
120
160
200
240
180 135W 90W
-2 -1.5 -1 -0.5 0 0.5 1 1.5 2
(i) May uw, omega 5S:5N
(j) Dec uw, omega 5S:5N
hPa
150
200
250
300
400
500
700
850
1000
60E 120E 180 120W
-4.5 -3 -1.5 0 1.5 3 4.5

Figure 1.

The composite difference fields of the SST and SWS from March to December between nine strong positive SWSD years (1982, 1986, 1989, 1992, 1997, 2005, 2009, 2012, and 2014) and eight strong negative SWSD years (1980, 1984, 1988, 1990, 2002, 2006, 2007, and 2010) based on the ±0.7 standard deviations are provided (Figures 1e, 1f, and S4 in the Supporting Information S1). It is evident that weak negative SSTAs appear over the equatorial central-eastern Pacific in March, and transit to the weak positive SSTAs in April (Figures S4a and S4b in the Supporting Information S1). It is in May the positive SSTAs become significant when intensive surface westerly wind anomalies appear over the tropical western Pacific (Figures 1e and S4c in the Supporting Information S1). Due to the Bjerknes positive feedback (Bjerknes, 1969), the positive SSTAs and surface westerly wind anomalies would be further strengthened. Thus, May is the key month in the process of how SWS dipole mode influences El Niño events. This conclusion is consistent when the criterions are ±0.8 and ±1.0 standard deviations of SWSD.

The surface westerly wind anomalies over the tropical western Pacific in May stimulate the eastward-propagating Kelvin waves, which deepen the thermocline depth of the equatorial central-eastern Pacific, suppress the ocean upwelling, and then increase the SST in situ (Figures 1g and S5 in the Supporting Information S1). Furthermore, the surface westerly wind anomalies over the tropical western Pacific in May transport warm SST and abundant warm and humid flow from the tropical western Pacific to the central-eastern Pacific through the eastward of sea surface currents, which contribute to the occurrence of low-level convergences and deep convections over the central-eastern Pacific (Figures 1i and S6 in the Supporting Information S1). Thus, a typical opposite Walker circulation prevails in the tropical Pacific, which is characterized by ascending motions in the tropical central-eastern Pacific and descending motions in the western Pacific (Figures 1i and S6 in the Supporting Information S1). This typical atmospheric circulation is conducive to the further strengthening of the surface westerly wind anomalies over the tropical western Pacific, resulting in the occurrence of El Niño events in the subsequent winter via the Bjerknes positive feedback (Figures 1f, 1h, 1j, and S4–S6 in the Supporting Information S1).

In a word, the composite differences between strong positive and negative SWSD years reveal that intensive surface westerly wind anomalies occur over the tropical western Pacific in May, which would stimulate the subsequent winter El Niño events. However, how do the surface westerly wind anomalies in May arise? This process is further investigated.

3.2. Features of Spring SWS Dipole Mode Over the TP

First of all, we present the local features of atmospheric circulations associated with SWS diploe mode in May. The composite differences show that the southwesterly wind anomalies prevail over the southern TP with easterly wind anomalies occupying the western and northern part (Figure 2a). Correspondingly, the positive SH anomalies dominate the southern part, and negative SH anomalies occupy the western and northern TP (Figure 2a). The SWS dipole mode over the TP is closely connected with anomalous cyclone at 500 hPa (Figure 2c), which is a part of the baroclinic structure with anomalous low-level anticyclones and mid–high-level cyclones over the western TP (Figure 2b). In previous study, we revealed that the winter–spring North Atlantic tripole SSTAs could trigger the downstream-propagating Rossby waves, and further induce the spring baroclinic structure over the western TP (Yu et al., 2021).

On the southeastern flank of the cyclones, the southwesterly flows (700–500 hPa) carry abundant water vapors from the Arabian Sea, which ascend along the slope of the southwestern TP and result in convergences and ascending movements in situ (Figures S7a and S7b in the Supporting Information S1). Subsequently, positive precipitation anomalies appear over the western TP (Figure 2d), leading to the decrease of Ts and Ts–Ta (Figure S7c

Figure 1. (a) The spatial pattern of the second empirical orthogonal function mode of spring SWS over the Tibetan Plateau above 2,000 m. The value in the upper right is the explained variance. (b) Time series of the normalized surface wind speed dipole (SWSD) (red solid curve) and SWSPC2 (blue solid curve). The solid horizontal lines represent ±0.7 standard deviations. Correlation patterns between the following autumn sea surface temperature (SST) (c), the following winter SST (d), and spring SWSD. Composite differences between strong positive and negative SWSD years. SST (shading, °C) and surface wind (vectors, m s^{-1}) in May (e) and December (f). Vertical cross-section of ocean potential temperature (°C) averaged between 5°S and 5°N in May (g) and December (h). The green and black solid lines represent the anomalous and climatological thermocline depth, respectively. Vertical cross-section of zonal circulation (vectors, m s^{-1}; vertical speed is scaled by 200 to facilitate visualization) and vertical velocity (0.005 Pa s^{-1}) are averaged between 5°S and 5°N in May (i) and December (j). The stippled areas in (c) and (d) denote values exceeding the 95% confidence level. The stippled areas in (e–h), the shading in (i and j), the red vectors in (e and f), and the black vectors in (i and j) denote values exceeding the 90% confidence level.

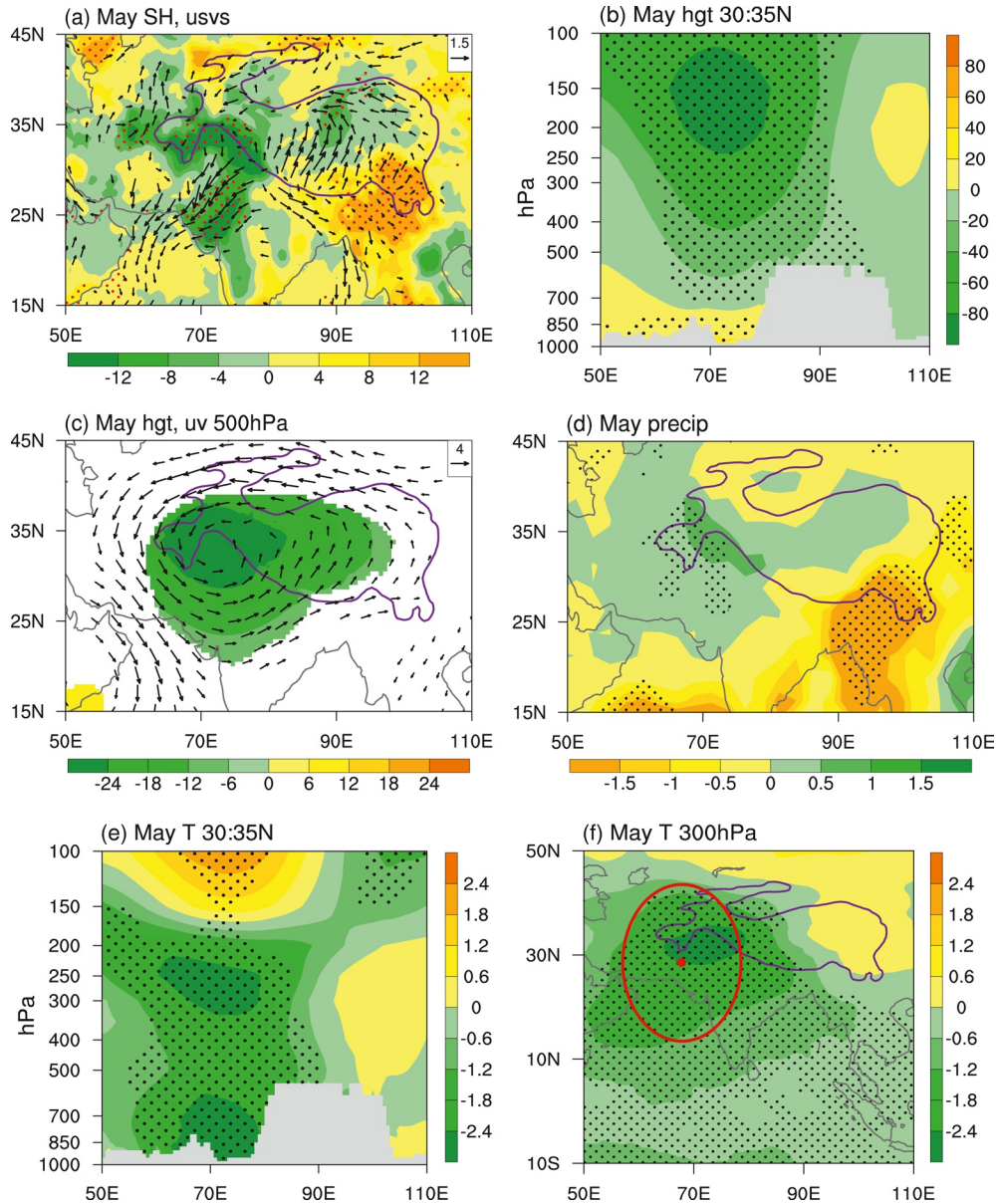

Figure 2. Composite differences between strong positive and negative surface wind speed dipole years in May. (a) Surface sensible heating (shading, W m^{-2}) and surface wind (vectors, m s^{-1}). (b) Vertical cross-section of geopotential height (gpm) averaged between 30° and 35°N. (c) 500 hPa geopotential height (shading, gpm) and wind (vectors, m s^{-1}). (d) Precipitation (mm d^{-1}). (e) Vertical cross-section of air temperature (°C) averaged between 30° and 35°N. (f) 300 hPa air temperature (°C). The stippled areas in (a and b), and (d–f), the shading in (c), and the black vectors in (a and c) denote values exceeding the 95% confidence level.

in the Supporting Information S1). Based on the bulk aerodynamic formula, the SH would further decrease over the western TP. The negative SH anomalies can also induce the baroclinic structure with anomalous low-level anticyclones and mid–high-level cyclones according to the thermal adapted theory (Wu & Liu, 2000). That is, there exists a positive feedback between the negative SH anomalies and the baroclinic structure over the western TP, which is called a "negative SH–baraclinic structure" (Yu et al., 2021).

We further examine the air temperature (T) features corresponding to the "negative SH–baraclinic structure". Based on the static equilibrium ($\partial\Phi'/\partial z \propto T'$), the vertical variation of the geopotential height (Φ) anomalies are positively related to the T anomalies (L. Wang et al., 2017). The baroclinic structure over the western TP is characterized by low-level positive Φ anomalies and mid–high-level negative Φ anomalies. Thus, the vertical

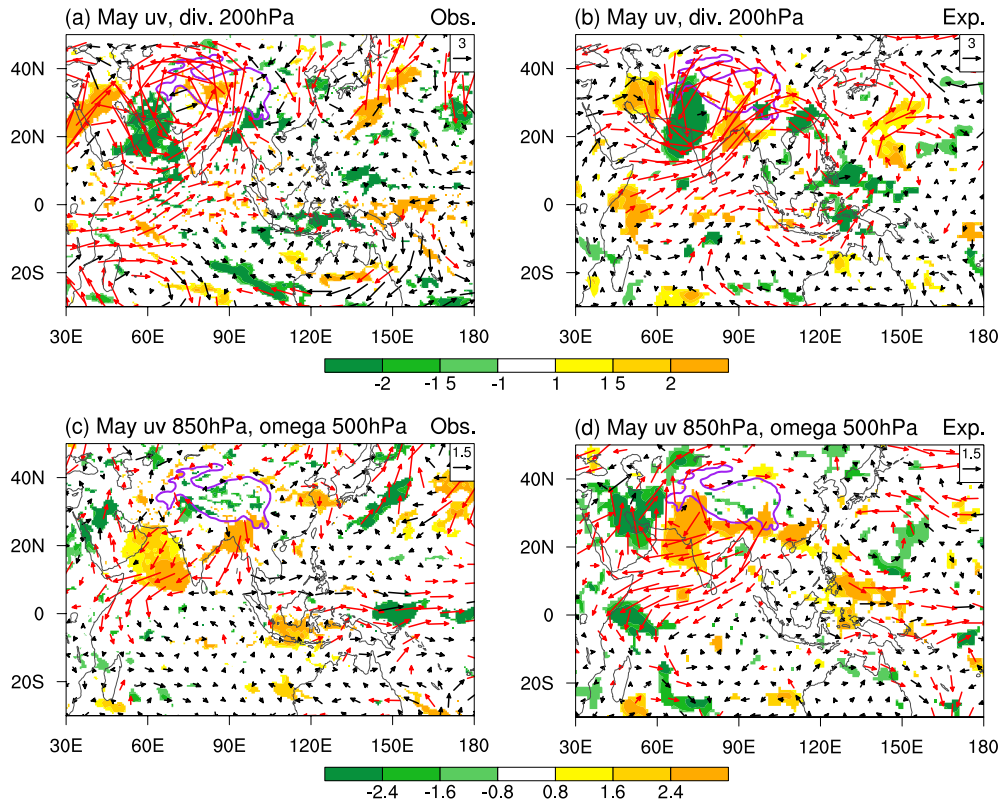

Figure 3. Composite differences between strong positive and negative surface wind speed dipole years in May. (a) 200 hPa wind (vectors, m s^{-1}) and its divergence (shading, 10^{-6} s^{-1}). (c) 850 hPa wind (vectors, m s^{-1}) and 500 hPa vertical velocity (0.01 Pa s^{-1}). (b and d) Same as (a and c), respectively, but for differences between TP–T and control run ensemble means in May. The shading and the red vectors in (a–d) denote values exceeding the 90% confidence level.

T anomalies are negative with two cold centers at the near surface and around 300 hPa in situ, respectively (Figure 2e). In horizonal direction, the high-level cold center is also located over the western TP (Figure 2f). The sensitivity experiments are forced by the three-dimensional *T* anomalies in May. Detailed designs of experiments are given in Section 2.3.

3.3. Underlying Physical Mechanisms of How Spring SWS Dipole Mode Over the TP Affects the Subsequent Winter ENSO Events

Firstly, we explore the underlying physical mechanisms of how the positive SWS dipole mode over the TP affects the surface westerly wind anomalies over the tropical western Pacific in May. In the observations, accompanying with the "negative SH–baroclinic structure", low pressure anomalies at high level occupy the western TP–India regions, which can induce the southwesterly wind anomalies over the tropical western Indian Ocean via the pressure gradient force (Figure 3a). The tropical westerly wind anomalies over the Indian Ocean gradually decrease from the west to the east, then the high-level horizontal convergences and descending motions appear over the Maritime Continent (Figures 3a and 3c). Thus, the surface westerly wind anomalies prevail over the tropical western Pacific owing to the low-level divergences (Figure 3c). These anomalous circulations in the equatorial Indian Ocean and western Pacific show the opposite direction to the climatology circulations in May (Figure S9 in the Supporting Information S1), but bear strong resemblance to the negative rotation of the GIP (Meng & Wu, 2000; Wu & Meng, 1998). Therefore, the high-level westerly wind anomalies over the equatorial Indian Ocean can induce the surface westerly wind anomalies over the equatorial western Pacific via the negative rotation of the GIP.

In numerical experiments, the baroclinic structure with low-level anomalous anticyclones and high-level anomalous cyclones over the western TP–Indian Ocean are well reproduced (Figures 3b and 3d). The anomalous westerly winds appear over the equatorial Indian Ocean at a high level. Based on the GIP theory, descending motions and low-level divergences appear over the Maritime Continent, and then the anomalous surface westerly winds develop in the equatorial western Pacific. The intensity of this GIP process is close to that in the observations.

In addition, the "negative SH–baroclinic structure" over the western TP can stimulate downstream-propagating Rossby waves from the western TP to the central North Pacific both in the observations and numerical experiments (Figures 4a, 4b, and S8b in the Supporting Information S1). The Rossby waves result in the equivalent barotropic low pressure anomalies over the central North Pacific (Figures 4a–4d). Then surface anomalous cyclonic circulation appears in the central North Pacific, accompanied by southwesterly wind anomalies to its southeast, which is marked "A" in the observations (Figure 4c) and "B" in the experiments (Figure 4d). The southwesterly wind anomalies weaken the Pacific northeast trade winds. According to the wind–evaporation–SST feedback (Xie & Philander, 1994), the weakened northeast trade winds weaken the evaporation, which would further reduce the heat flux from the ocean to the atmosphere. Thus, the downward latent heat and net heat flux increase (Figures 4g–4j), and positive SSTAs appear in region A (B) in the observations (experiments) during May (Figures 4c and 4d). As the anomalous cyclone over the central North Pacific exists only in May and June, the positive SSTAs in region A (region B) in the observations (experiments) are also significant in May and June (Figures 4e and 4f). This positive SSTAs in the observations are stronger and farther north than that in the experiments. Furthermore, this positive SSTAs over the subtropical Pacific force the atmospheric circulation and induce the surface westerly wind anomalies over the equatorial western Pacific through the so–called SFM process both in the observations and the experiments (Figures 4c–4f) (Vimont et al., 2001, 2003). Finally, the El Niño events occur in the subsequent winter via the Bjerknes positive feedback both in the observations and the experiments (Figures S4 and S10 in the Supporting Information S1).

In the experiments, the intensity of May GIP process is comparable with that in the observations (Figure 3), but the intensity of May SFM process is weaker than that in the observations (Figure 4). And the May surface westerly wind anomalies over the equatorial western Pacific induced by these two processes are comparable between the observations and the experiments. Thus, we infer that the GIP process may be more important than the SFM process for the intensification of surface westerly wind anomalies in May.

4. Conclusions and Further Discussion

4.1. Conclusions

The potential impacts of the south–north dipole modes of spring SH and SWS over the TP on the subsequent winter ENSO events are explored in this study. During the positive phase of spring SWS dipole mode over the TP, easterly (southwesterly) wind anomalies and negative (positive) SH anomalies appear over the western and northern (southern) TP. The effect of the SWS is amplified due to the local positive feedback between SH, precipitation, and circulation over the western TP during May, which forms a "negative SH–baroclinic structure".

Accompanying with the "negative SH–baroclinic structure", anomalous high-level low pressures over the western TP–India could cause westerly wind anomalies over the equatorial Indian Ocean, which result in convergences over the Maritime Continent. Thus, the surface westerly wind anomalies occur in the tropical western Pacific via the GIP process. In addition, the "negative SH–baroclinic structure" stimulates the downstream-propagating Rossby waves to the central North Pacific, leading to the anomalous surface cyclone in situ. This anomalous surface cyclone induces southwesterly wind anomalies over its southeast, which weakens the northeast trade winds and warms the local SST via wind–evaporation–SST feedback. Then this positive SSTAs induce surface westerly wind anomalies over the tropical western Pacific via the SFM process, which may be less important than the GIP process. The surface westerly wind anomalies over the tropical western Pacific induced by the GIP and SFM processes trigger eastward-propagating Kelvin waves, resulting in deepened thermocline depth and positive SSTAs over the equatorial central-eastern Pacific. Subsequently, the surface westerly wind anomalies and positive SSTAs further develop via the Bjerknes positive feedback, and El Niño events occur in the following winter. These physical processes are well captured in the numerical sensitivity experiments, although the simulated El Niño events are slightly weaker.

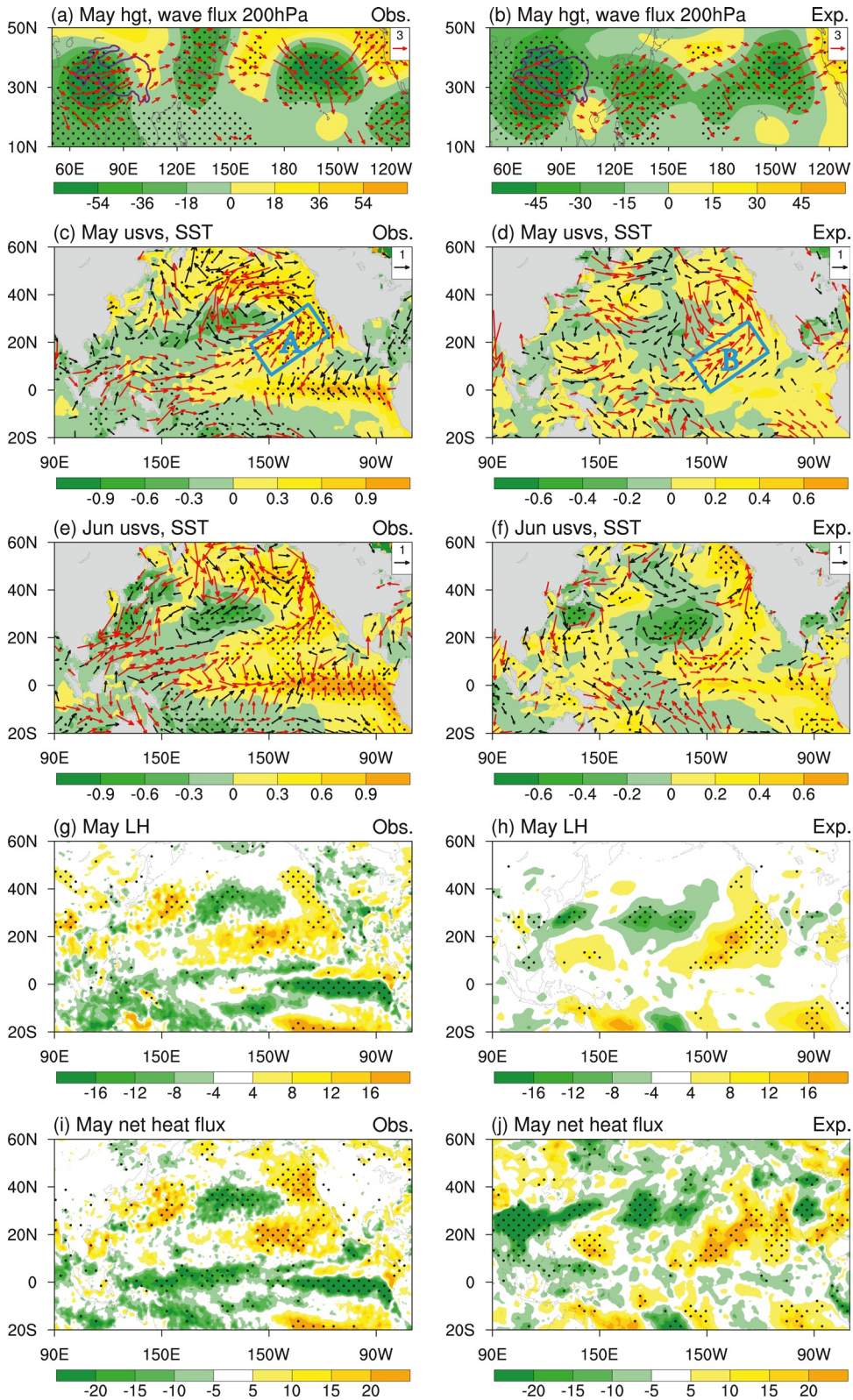

Figure 4. Composite differences between strong positive and negative surface wind speed dipole years. (a) 200 hPa geopotential height (shading, gpm) and stationary wave activity flux (vectors, $m^2\ s^{-2}$) in May. Sea surface temperature (shading, °C) and surface wind (vectors, $m\ s^{-1}$) in May (c) and June (e). (g) Downward latent heat ($W\ m^{-2}$). (i) Downward net heat flux ($W\ m^{-2}$). (b, d, f, h, and j) Same as (a, c, e, g, and i), respectively, but for differences between TP–T and control run ensemble means. The stippled areas in (a–j) and the red vectors in (c–f) denote values exceeding the 90% confidence level.

4.2. Further Discussion

The conclusions are reached in the composite difference between the positive and negative phases of the SWS dipole mode. Whether the negative phase of spring SWS dipole mode could also stimulate the La Niña events is further discussed. During the negative phase of spring SWS dipole mode over the TP, there is positive SH anomalies (Figure S11a in the Supporting Information S1), negative precipitation anomalies (Figure S11d in the Supporting Information S1), high pressure anomalies at mid–high level and low pressure anomalies at low level over the western TP in May (Figures S11b and S11c in the Supporting Information S1). This "positive SH–baroclinic structure" can induce the surface easterly anomalies over the tropical western Pacific in May (Figure S12c in the Supporting Information S1). Thus, the significant negative SSTAs appear over the tropical central-eastern Pacific since May, and the La Niña events appear in the following winter (Figure S12 in the Supporting Information S1). Besides, the strength of La Niña events induced by the negative phase of SWS dipole mode (Figure S12 in the Supporting Information S1) is weaker than the El Niño events induced by the positive phase of SWS dipole mode (Figure S13 in the Supporting Information S1).

According to the Niño3 index and El Niño Modoki index (the two indices are often selected to represent the Eastern-Pacific ENSO and Central-Pacific ENSO, respectively, Ashok et al., 2007), we find that the Eastern-Pacific ENSO would occur more frequently with the spring SWS dipole mode forcing over the TP than the Central-Pacific ENSO in observations and numerical experiments (Figures S4 and S10 in the Supporting Information S1).

Although the impact of preceding winter ENSO events on the spring thermal anomalies over the TP is insignificantly in terms of the statistical relationship, there indeed exists some years that the spring thermal anomalies over the TP are closely related to the preceding winter ENSO events. There are asymmetric relationships between preceding winter ENSO and spring SWSD, and between spring SWSD and succeeding winter ENSO, which need a further study. Moreover, in nine positive SWSD years, there are five succeeding winter El Niño events, among which only one El Niño event corresponds to a La Niña event in the preceding winter. In eight negative SWSD years, there are four succeeding winter La Niña events, among which three preceding winters are El Niño events. How the preceding winter ENSO events modulate the spring thermal forcing over the TP and further affect the succeeding winter ENSO events? This issue still warrants a further investigation.

Recently, the three-ocean interactions have gain popularities in the field of meteorology, which is benificial for an in-depth underatanding of climate change over the global region (C. Z. Wang, 2019). The spring SWS dipole mode over the TP and preceding winter–spring North Atlantic tripole SSTAs are significantly connected (Figure S14 in the Supporting Information S1). The correlation coefficient between the winter–spring North Atlantic tripole SSTAs index (defined by Yu et al., 2021) and subsequent winter Niño3.4 index is significant (0.34, $p < 0.05$). However, after removing the spring SWS dipole mode effect, the partial correlation coefficient is insignificant (0.1, $p > 0.1$). Thus, the spring SWS dipole mode might provide an intermediate bridge effect in linking the North Atlantic tripole SSTAs and ENSO events, which should be further investigated in later studies.

Data Availability Statement

The MERRA-2 reanalysis data is downloaded from https://gmao.gsfc.nasa.gov/GMAO_products/reanalysis_products.php. The GPCP precipitation data is downloaded from https://www.esrl.noaa.gov/psd/data/gridded/data.gpcp.html. The HadISST1 data is obtained from https://www.metoffice.gov.uk/hadobs/hadisst/. The GODAS data is obtained from http://www.esrl.noaa.gov/psd/data/gridded/data.godas.html. The model data is available at https://doi.org/10.5281/zenodo.6084926.

Acknowledgments
We thank the editor, two anonymous reviewers, Dr. Tuantuan Zhang, and Dr. Ziqian Wang for their constructive and helpful comments. This work was jointly supported by the National Natural Science Foundation of China (91937302), the Guangdong Major Project of Basic and Applied Basic Research (2020B0301030004), the Strategic Priority Research Program (XDB40030200) and the National Natural Science Foundation of China (41730963, 42105062, 42175023, and 41975080).

References

Adler, R. F., Huffman, G. J., Chang, A., Ferraro, R., Xie, P. P., Janowiak, J., et al. (2003). The version-2 global precipitation climatology project (GPCP) monthly precipitation analysis (1979-present). *Journal of Hydrometeorology*, *4*(6), 1147–1167. https://doi.org/10.1175/1525-7541(2003)004<1147:tvgpcp>2.0.co;2

Alexander, M. A., Blade, I., Newman, M., Lanzante, J. R., Lau, N. C., & Scott, J. D. (2002). The atmospheric bridge: The influence of ENSO teleconnections on air-sea interaction over the global oceans. *Journal of Climate*, *15*(16), 2205–2231. https://doi.org/10.1175/1520-0442(2002)015<2205:tabtio>2.0.co;2

Ashok, K., Behera, S. K., Rao, S. A., Weng, H. Y., & Yamagata, T. (2007). El Niño Modoki and its possible teleconnection. *Journal of Geophysical Research: Oceans*, *112*, C11007. https://doi.org/10.1029/2006jc003798

Bao, Q., Lin, P. F., Zhou, T. J., Liu, Y. M., Yu, Y. Q., Wu, G. X., et al. (2013). The flexible Global Ocean-Atmosphere-Land system model, spectral version 2: FGOALS-s2. *Advances in Atmospheric Sciences*, *30*(3), 561–576. https://doi.org/10.1007/s00376-012-2113-9

Bao, Q., Wu, X. F., Li, J. X., Wang, L., He, B., Wang, X. C., et al. (2019). Outlook for El nino and the Indian ocean dipole in autumn-winter 2018-2019 (in Chinese). *Chinese Science Bulletin*, *64*(1), 73–78. https://doi.org/10.1360/n972018-00913

Behringer, D., & Xue, Y. (2004). Evaluation of the global ocean data assimilation system at NCEP: The Pacific Ocean. In *Eighth symposium on integrated observing and assimilation systems for atmosphere, oceans, and land surface* (Vol. 3). AMS 84th Annual Meeting. https://ams.confex.com/ams/84Annual/techprogram/paper_70720.htm

Bjerknes, J. (1969). Atmospheric teleconnections from the equatorial Pacific. *Monthly Weather Review*, *97*(3), 163–172. https://doi.org/10.1175/1520-0493(1969)097<0163:atftep>2.3.co;2

Duan, A. M., & Wu, G. X. (2005). Role of the Tibetan Plateau thermal forcing in the summer climate patterns over subtropical Asia. *Climate Dynamics*, *24*(7–8), 793–807. https://doi.org/10.1007/s00382-004-0488-8

Duan, A. M., & Wu, G. X. (2008). Weakening trend in the atmospheric heat source over the Tibetan Plateau during recent decades. Part I: Observations. *Journal of Climate*, *21*(13), 3149–3164. https://doi.org/10.1175/2007jcli1912.1

Duchon, C. E. (1979). Lanczos filtering in one and two dimensions. *Journal of Applied Meteorology*, *18*(8), 1016–1022. https://doi.org/10.1175/1520-0450(1979)018<1016:lfioat>2.0.co;2

Eisenman, I., Yu, L. S., & Tziperman, E. (2005). Westerly wind bursts: ENSO's tail rather than the dog? *Journal of Climate*, *18*(24), 5224–5238. https://doi.org/10.1175/jcli3588.1

Fedorov, A. V., Hu, S. N., Lengaigne, M., & Guilyardi, E. (2015). The impact of westerly wind bursts and ocean initial state on the development, and diversity of El Niño events. *Climate Dynamics*, *44*(5–6), 1381–1401. https://doi.org/10.1007/s00382-014-2126-4

Gelaro, R., McCarty, W., Suarez, M. J., Todling, R., Molod, A., Takacs, L., et al. (2017). The Modern-Era retrospective analysis for Research and Applications, version 2 (MERRA-2). *Journal of Climate*, *30*(14), 5419–5454. https://doi.org/10.1175/jcli-d-16-0758.1

Guilyardi, E. (2006). El Niño-mean state-seasonal cycle interactions in a multi-model ensemble. *Climate Dynamics*, *26*(4), 329–348. https://doi.org/10.1007/s00382-005-0084-6

He, B., Bao, Q., Wang, X. C., Zhou, L. J., Wu, X. F., Liu, Y. M., et al. (2019). CAS FGOALS-f3-L model datasets for CMIP6 historical atmospheric model Intercomparison project simulation. *Advances in Atmospheric Sciences*, *36*(8), 771–778. https://doi.org/10.1007/s00376-019-9027-8

He, S. C., Yang, J., Bao, Q., Wang, L., & Wang, B. (2019). Fidelity of the observational/reanalysis datasets and global climate models in representation of extreme precipitation in east China. *Journal of Climate*, *32*(1), 195–212. https://doi.org/10.1175/jcli-d-18-0104.1

Jin, F. F. (1997). An equatorial ocean recharge paradigm for ENSO. Part I: Conceptual model. *Journal of the Atmospheric Sciences*, *54*(7), 811–829. https://doi.org/10.1175/1520-0469(1997)054<0811:aeorpf>2.0.co;2

Knutson, T. R., Manabe, S., & Gu, D. F. (1997). Simulated ENSO in a global coupled ocean-atmosphere model: Multidecadal amplitude modulation and CO_2 sensitivity. *Journal of Climate*, *10*(1), 138–161. https://doi.org/10.1175/1520-0442(1997)010<0138:seiagc>2.0.co;2

Latif, M., Sterl, A., Maierreimer, E., & Junge, M. M. (1993). Structure and predictability of the El Niño/Southern Oscillation phenomenon in a coupled ocean-atmosphere general circulation model. *Journal of Climate*, *6*(4), 700–708. https://doi.org/10.1175/1520-0442(1993)006<0700:sapote>2.0.co;2

Li, J. X., Bao, Q., Liu, Y. M., Wu, G. X., Wang, L., He, B., et al. (2019). Evaluation of FAMIL2 in simulating the climatology and seasonal-to-interannual variability of tropical cyclone characteristics. *Journal of Advances in Modeling Earth Systems*, *11*(4), 1117–1136. https://doi.org/10.1029/2018ms001506

Lian, T., Chen, D. K., Tang, Y. M., & Wu, Q. Y. (2014). Effects of westerly wind bursts on El Niño: A new perspective. *Geophysical Research Letters*, *41*(10), 3522–3527. https://doi.org/10.1002/2014gl059989

Liu, Y. M., Bao, Q., Duan, A. M., Qian, Z. A., & Wu, G. X. (2007). Recent progress in the impact of the Tibetan Plateau on climate in China. *Advances in Atmospheric Sciences*, *24*(6), 1060–1076. https://doi.org/10.1007/s00376-007-1060-3

Liu, Y. M., Lu, M. M., Yang, H. J., Duan, A. M., He, B., Yang, S., & Wu, G. X. (2020). Land-atmosphere-ocean coupling associated with the Tibetan Plateau and its climate impacts. *National Science Review*, *7*(3), 534–552. https://doi.org/10.1093/nsr/nwaa011

McPhaden, M. J. (1999). Genesis and evolution of the 1997-98 El Niño. *Science*, *283*(5404), 950–954. https://doi.org/10.1126/science.283.5404.950

McPhaden, M. J., Zebiak, S. E., & Glantz, M. H. (2006). ENSO as an integrating concept in Earth science. *Science*, *314*(5806), 1740–1745. https://doi.org/10.1126/science.1132588

Meng, W., & Wu, G. X. (2000). Gearing between the indo-monsoon circulation and the Pacific-walker circulation and the ENSO. Part II: Numerical simulation (in Chinese). *Chinese Journal of Atmospheric Sciences*, *24*(1), 15–25.

Nan, S. L., Zhao, P., Yang, S., & Chen, J. M. (2009). Springtime tropospheric temperature over the Tibetan Plateau and evolutions of the tropical Pacific SST. *Journal of Geophysical Research: Atmospheres*, *114*, D10104. https://doi.org/10.1029/2008jd011559

Rayner, N. A., Parker, D. E., Horton, E. B., Folland, C. K., Alexander, L. V., Rowell, D. P., et al. (2003). Global analyses of sea surface temperature, sea ice, and night marine air temperature since the late nineteenth century. *Journal of Geophysical Research: Atmospheres*, *108*(D14), 4407. https://doi.org/10.1029/2002jd002670

Schopf, P. S., & Suarez, M. J. (1988). Vacillations in a coupled ocean-atmosphere model. *Journal of the Atmospheric Sciences*, *45*(3), 549–566. https://doi.org/10.1175/1520-0469(1988)045<0549:viacom>2.0.co;2

Sun, R. Z., Duan, A. M., Chen, L. L., Li, Y. J., Xie, Z., & Zhao, Y. (2019). Interannual variability of the north Pacific mixed layer associated with the spring Tibetan Plateau thermal forcing. *Journal of Climate*, *32*(11), 3109–3130. https://doi.org/10.1175/jcli-d-18-0577.1

Takaya, K., & Nakamura, H. (2001). A formulation of a phase-independent wave-activity flux for stationary and migratory quasi-geostrophic eddies on a zonally varying basic flow. *Journal of the Atmospheric Sciences*, *58*(6), 608–627. https://doi.org/10.1175/1520-0469(2001)058<0608:afoapi>2.0.co;2

Trenberth, K. E. (1997). The definition of El Niño. *Bulletin of the American Meteorological Society*, *78*(12), 2771–2777. https://doi.org/10.1175/1520-0477(1997)078<2771:tdoeno>2.0.co;2

Vimont, D. J., Battisti, D. S., & Hirst, A. C. (2001). Footprinting: A seasonal connection between the tropics and mid-latitudes. *Geophysical Research Letters*, *28*(20), 3923–3926. https://doi.org/10.1029/2001gl013435

Vimont, D. J., Wallace, J. M., & Battisti, D. S. (2003). The seasonal footprinting mechanism in the Pacific: Implications for ENSO. *Journal of Climate*, *16*(16), 2668–2675. https://doi.org/10.1175/1520-0442(2003)016<2668:tsfmit>2.0.co;2

Wang, B., Bao, Q., Hoskins, B., Wu, G. X., & Liu, Y. M. (2008). Tibetan plateau warming and precipitation changes in East Asia. *Geophysical Research Letters*, *35*, L14702. https://doi.org/10.1029/2008gl034330

Wang, B., Wu, R. G., & Fu, X. H. (2000). Pacific-East Asian teleconnection: How does ENSO affect east Asian climate? *Journal of Climate*, *13*(9), 1517–1536. https://doi.org/10.1175/1520-0442(2000)013<1517:peathd>2.0.co;2

Wang, C. Z. (2001). A unified oscillator model for the El Niño-Southern Oscillation. *Journal of Climate*, *14*(1), 98–115. https://doi.org/10.1175/1520-0442(2001)014<0098:auomft>2.0.co;2

Wang, C. Z. (2019). Three-ocean interactions and climate variability: A review and perspective. *Climate Dynamics*, *53*(7–8), 5119–5136. https://doi.org/10.1007/s00382-019-04930-x

Wang, L., Xu, P. Q., Chen, W., & Liu, Y. (2017). Interdecadal variations of the silk road pattern. *Journal of Climate*, *30*(24), 9915–9932. https://doi.org/10.1175/jcli-d-17-0340.1

Weisberg, R. H., & Wang, C. Z. (1997). A Western Pacific oscillator paradigm for the El Niño southern oscillation. *Geophysical Research Letters*, *24*(7), 779–782. https://doi.org/10.1029/97gl00689

Wen, Q., Döös, K., Lu, Z. Y., Han, Z. X., & Yang, H. J. (2020). Investigating the role of the Tibetan Plateau in ENSO variability. *Journal of Climate*, *33*(11), 4835–4852. https://doi.org/10.1175/jcli-d-19-0422.1

Wu, G. X., Li, W. P., & Guo, H. (1997). Sensible heat driven air-pump over the Tibetan Plateau and its impacts on the Asian summer monsoon (in Chinese). *Collections on the memory of Zhao Jiuzhang*, (pp. 116–126). Chinese Science Press.

Wu, G. X., & Liu, Y. M. (2000). Thermal adaptation, overshooting, dispersion, and subtropical high. Part I: Thermal adaptation and overshooting (in Chinese). *Chinese Journal of Atmospheric Sciences*, *24*(4), 433–436.

Wu, G. X., Liu, Y. M., Wang, T. M., Wan, R. J., Liu, X., Li, W. P., et al. (2007). The influence of mechanical and thermal forcing by the Tibetan Plateau on Asian climate. *Journal of Hydrometeorology*, *8*(4), 770–789. https://doi.org/10.1175/jhm609.1

Wu, G. X., & Meng, W. (1998). Gearing between the indo-monsoon circulation and the Pacific-walker circulation and the ENSO. Part I: Data analyses (in Chinese). *Chinese Journal of Atmospheric Sciences*, *22*(4), 470–480.

Wyrtki, K. (1985). Water displacements in the Pacific and the Genesis of El Niño cycles. *Journal of Geophysical Research: Oceans*, *90*(NC4), 7129–7132. https://doi.org/10.1029/jc090ic04p07129

Xie, S. P., & Philander, S. G. H. (1994). A coupled ocean-atmosphere model of relevance to the ITCZ in the eastern Pacific. *Tellus Series a-Dynamic Meteorology and Oceanography*, *46*(4), 340–350. https://doi.org/10.3402/tellusa.v46i4.15484

Yu, W., Liu, Y. M., Yang, X. Q., & Wu, G. X. (2018). The interannual and decadal variation characteristics of the surface sensible heating at different elevations over the Qinghai-Tibetan Plateau and Attribution analysis (in Chinese). *Plateau Meteorology*, *37*(5), 1161–1176.

Yu, W., Liu, Y. M., Yang, X. Q., Wu, G. X., He, B., Li, J. X., & Bao, Q. (2021). Impact of North Atlantic SST and Tibetan Plateau forcing on seasonal transition of springtime South Asian monsoon circulation. *Climate Dynamics*, *56*(1–2), 559–579. https://doi.org/10.1007/s00382-020-05491-0

Zhao, P., Zhu, Y. N., & Zhang, R. H. (2007). An Asian-Pacific teleconnection in summer tropospheric temperature and associated Asian climate variability. *Climate Dynamics*, *29*(2–3), 293–303. https://doi.org/10.1007/s00382-007-0236-y

Zhao, Y., Duan, A. M., & Wu, G. X. (2018). Interannual variability of late-spring circulation and diabatic heating over the Tibetan plateau associated with Indian ocean forcing. *Advances in Atmospheric Sciences*, *35*(8), 927–941. https://doi.org/10.1007/s00376-018-7217-4